

# Non-linear control for enhanced solar power under partial shading and AC load variations

Sabri Khadija, El Maguiri Ouadia, Farchi Abdelmajid

Department of Electrical and Mechanical Engineering, IMMII-lab, Faculty of Science and Technology, University Hassan 1<sup>st</sup>, Settat, Morocco

## Article Info

### Article history:

Received Nov 25, 2023

Revised Jan 9, 2024

Accepted Jan 11, 2024

### Keywords:

AC load

Backstepping control

DC link

Grid-connected

MPPT

Partial shading

PSO

## ABSTRACT

This paper solves the control problem to track the maximum power in grid-connected PV systems to catch up with the changes and meet the energy demand, given the irregular and arbitrary nature of the solar source. Our work addresses the following objectives: i) extracting the maximum available power under partial shading, ii) and having a unit power factor. To achieve the above objectives, we have integrated two control components. The first one is dedicated to the extraction of the maximum power point (MPPT) particle swarming algorithm (PSO) with a backstepping controller, by shaking on the DC/DC converter duty cycle to increase the robustness and stability of the system. The backstepping control of the three-phase voltage source inverter is the second part. To verify the effectiveness of the introduced system, modelling and simulation are verified in MATLAB/Simulink.

*This is an open access article under the [CC BY-SA](https://creativecommons.org/licenses/by-sa/4.0/) license.*



## Corresponding Author:

Sabri Khadija

Department of Electrical and Mechanical Engineering, IMMII-lab, Faculty of Science and Technology

University Hassan 1<sup>st</sup>

Settat, Morocco

Email: k.sabri@uhp.ac.ma

## 1. INTRODUCTION

Renewable energy sources (RES) have sparked widespread interest in recent decades as a means of ensuring rural electrification due to their numerous environmental benefits, low maintenance costs, long life, and abundant availability [1]. Solar and wind energy are known to be dependable, appealing, and cost-effective sources of energy when compared to other RES [2]. Today, all studies and research have been directed toward maximizing the utilization of the energy produced by PV panels either for use in low-power autonomous systems such as storage or pumping systems [3]–[6] or in grid-connected systems for high-power applications [7]–[9]. In general, the following objectives must be met to ensure a safe and reliable connection to the power grid despite climatic changes (temperature and irradiation) [2]: maximum power extraction (MPPT) from the PV, power factor correction, DC link voltage regulation, and total harmonic distortion (THD) minimization [8]. For this purpose, various robust and intelligent controllers have been proposed in the literature.

In our work, we proposed a dual-stage grid-connected PV system with an output LC filter [1], [10]–[12], as shown in Figure 1, which requires a DC/DC power converter as the link unit between the PV and the grid, unlike other types of single-stage systems [13], [14]. This paper presents a groundbreaking controller that uniquely integrates the PSO algorithm with backstepping control to optimize power extraction under partial shading conditions (PSC) while effectively addressing the system's non-linearity. The researchers [15]–[17], a DC/DC converter plays a crucial role in mitigating partial shading effects and

elevating PV voltage to a suitable level, enabling the effective utilization of various MPPT algorithms, both conventional and AI-based [17], [18]. Secondly, the three-phase inverter with a DC/AC voltage source is controlled by the backstepping controller to ensure energy processing between the PV panels and the electrical grid and compensate for the reactive power caused by the AC load to reduce the THD harmonic component, to keep the grid parameters at the desired values through power factor correction [19], [20].

Many studies have been conducted on grid-connected PV systems, each with its control strategies. Rivera *et al.* [21] proposes a three-phase single-stage grid-connected PV system with a Lyapunov-based nonlinear control strategy to achieve MPP with the INC algorithm and to control the active and reactive power of the DC/AC inverter to ensure a unity power factor (UPF) on the grid side, as well as in [22]. Meanwhile, Boujmil *et al.* [23] proposes a two-stage grid-connected PV system that is fully controlled by the nonlinear backstepping technique in his paper. The perturb and observe (P&O) algorithm is also used to investigate the maximization of reproduced energy from a solar power generation system. A hybrid system with photovoltaic (PV) and wind (WT) renewable generators with batteries is proposed by [24]. This system is coupled to an electrical grid in parallel with an alternative load via a flying capacitor inverter. The proposed control is based on the backstepping method and an energy management algorithm. Boujmil *et al.* [23] are focuses on a dynamic stability analysis of stand-alone hybrid DC microgrids using nonlinear countercurrent (NBC) controllers that are customized for different components of the microgrid such as a PV system, rectified diesel generator, loads, and a battery energy storage system. The countercurrent controller is designed to manage the power output of these components while reducing the incongruence between generation and consumption and maintaining a constant voltage on the DC bus, which serves as the main connection point for all microgrid components. A cascade control structure, as proposed in [25], [26], is employed to inject active and reactive power into a three-phase grid-connected solar PV system, accounting for external disturbances.

The work from Abouobaida [27] describes the analysis, modelling, and control of output voltages used to power DC and AC load systems. While controlling the output voltage, a ripple correlation current (RCC) algorithm and a back-stepping controller maximize the energy extracted from the PV generator. Saxena *et al.* [20] introduced a three-phase three-level diode inverter that controls active power in the grid using a synchronous reference frame technique. Except the three-level fixed neutral point inverter used in [9] manages its functions separately, and the maximum power control (MPPT) is based on an adaptive neuro-fuzzy inference system (ANFIS). Xie *et al.* [28], a nonlinear control function with DC bus hysteresis energy management is used in the external battery voltage loop. Karanayil *et al.* [29], the study aims to evaluate the performance of a three-phase grid-connected PV inverter. To reduce voltage ripples and keep the inverter running smoothly, the authors replaced the electrolytic capacitor with a low-value metallized polypropylene film capacitor. Most papers use PV/wind hybrid systems without the need for a storage system because the PV and wind systems complement each other. The power system's hybridization is depicted in [30]. In this groundbreaking work, we integrate an alternate load into our control strategy for grid-connected PV systems to maximize electricity, offering a flexible and all-encompassing response to the fluctuating demands of the energy market. To overcome the difficulties posed by partial shading, we integrate a backstepping controller with the particle swarm optimization (PSO) technique, which improves system resilience while preserving the UPF. This approach is used on the DC/DC converter and the control of the three-phase voltage source inverter. Its applicability is highlighted in situations where different loads can have a major impact on system performance through extensive modelling and simulations in MATLAB/Simulink. It is a grid-connected multi-source system (wind and PV).

We structure our work into four sections: section 2 addresses the modeling and configuration of a grid-connected PV system. In section 3, we delve into the proposed control strategy. Section 4 presents the simulation results obtained using MATLAB/Simulink. Finally, section 5 outlines perspectives and conclusions.

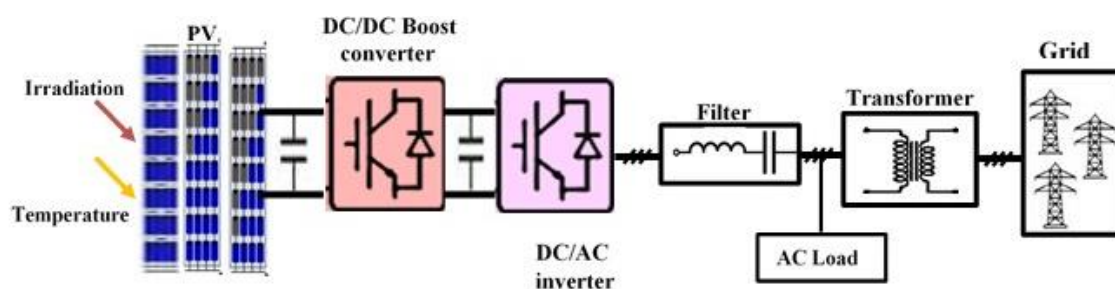


Figure 1. Diagram block of PV connected system and grid

**2. MODELING AND CONFIGURATION OF A GRID-CONNECTED PV SYSTEM**

The following section will delve into the mathematical modeling of the distinct components within the PV conversion chain. Figure 1 visually illustrates the comprehensive structure of the system, showcasing two specialized power stages dedicated to overseeing the distribution of PV power to the utility grid. This examination will provide insights into the precise functioning of each component, with a focus on optimizing the overall system performance.

**2.1. Partial shading conditions**

In practical scenarios, it is unusual for irradiation to remain uniform and constant at all times. Consequently, maximum power point (MPP) tracking becomes intricate when the entire PV array is subjected to PSC, as depicted in Figure 2, arising from factors such as clouds, birds, trees, and more. The power output of the PV system (SPV) diminishes because shaded cells act as loads and operate with an inverted voltage to match the current of unshaded cells [31]. This can lead to a hot-spot heating effect, potentially causing damage to the entire PV array [32]. In general, to mitigate these effects, a series of bypass diodes is installed in parallel on the PV module. These diodes are forward-biased to prevent localized energy dissipation at the shaded cells [33]. However, bypass diodes also introduce non-linear characteristics with multiple peak points in the characteristic curves. The number of these peak points is primarily associated with the quantity of PV modules connected in series within the PV array [34].

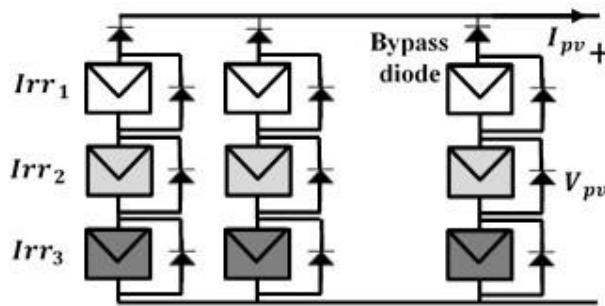


Figure 2. PV systems under different PSC

Figures 3 illustrate the output characteristics curve analysis (P-I) characteristics, offering a detailed analysis of the number of peak points. Output characteristics curve analysis; Figure 3(a) varied solar irradiance levels and Figure 3(b) performance under PSC Each peak point corresponds to specific incident irradiance levels on the panels, providing a comprehensive representation of the system's response to varying irradiation conditions.

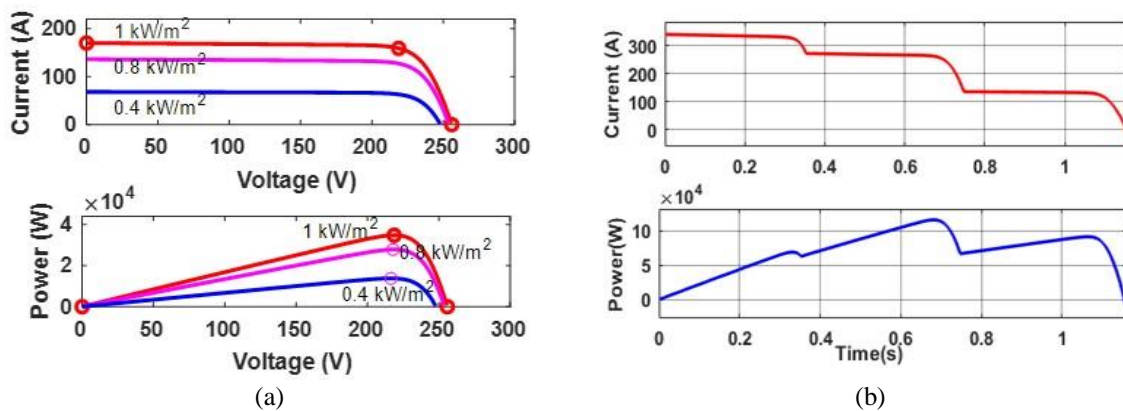


Figure 3. Output characteristics curve analysis for (a) varied solar irradiance levels and (b) performance under PSC

**2.2. Modeling the PV panel**

The synchronization of our PV system with the grid is depicted in Figure 4. This system comprises the following devices: a PV panel and a BOOST DC/DC converter, which adjusts the voltage of the PV panel to provide maximum MPPT power. This converter is connected to two bus capacitors that maintain a constant voltage on its input and output. Additionally, there is a three-phase voltage source inverter (DC/AC) that converts DC energy to AC energy, supplying either an AC load, the grid, or both. A three-phase LC filter is employed to reduce voltage ripples and achieve low THD. Finally, an isolation transformer is included in the system. The DC/AC is utilized to maintain the frequency and ensure that the current is in phase with the voltage, resulting in a UPF.

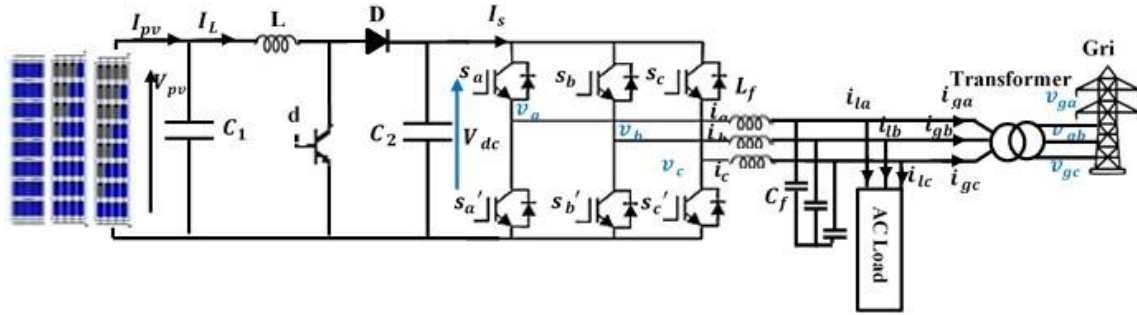


Figure 4. Interconnection of components in a three-phase grid-connected PV system

The efficiency of a PV module fluctuates with the incident light intensity. Therefore, it is crucial to examine the characteristics of a PV module under different irradiation scenarios, including uniform irradiation and PSC. In PSC, multiple local and global MPPs may appear on the P-V characteristics curve, as illustrated in Figure 3. The equivalent electrical circuit of a PV module is depicted in Figure 5 [35], [36].

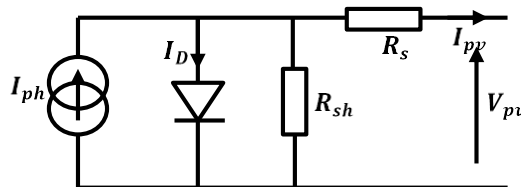


Figure 5. Equivalent circuit of a solar cell

The PV array module under consideration in this paper is the SPR-400E-WHT-D. The mathematical model for this circuit is based on the following equation:

$$I_{pv} = I_{ph} - I_s \left[ e^{\left( \frac{q(V_{pv} + I_{pv}R_s)}{AN_sKT} \right)} - 1 \right] - \frac{V_{pv} + I_{pv}R_s}{R_{sh}} \tag{1}$$

Where:

$$I_{ph} = [I_{ph0} + J_i(T - T_{sc})] \frac{E}{E_{sc}} \tag{2}$$

$$I_s = I_{s0} \left( \frac{T}{T_{sc}} \right)^3 e^{\frac{qE_{gp}}{AK} \left( \frac{1}{T_{sc}} - \frac{1}{T} \right)} \tag{3}$$

$$I_{s0} = \frac{I_{ph0}}{e^{\frac{qV_{oc}}{AKN_sT_{sc}} - 1}} \tag{4}$$

With:  $I_{ph}$ ,  $I_s$ , and  $I_{pv}$  denote the photo-current, saturation current, and PV panel current, respectively.  $V_{pv}$  is the PV panel voltage,  $N_s$  is the number of PV module cells,  $A$  is the ideality factor,  $K$  is the Boltzmann constant ( $1.3806503 \times 10^{-23}$  J/K),  $T$  is the cell temperature in Kelvin,  $q$  is the electron charge ( $1.60217646 \times 10^{-19}$  C),  $R_s$  is the series resistor,  $R_{sh}$  is the parallel resistor,  $E_{gap}$  is the bandgap energy of the PV cell semiconductor, equal to 1.12 eV.  $V_{oc}$  is the open-circuit voltage,  $I_{s0}$  is the saturation current at  $T_{sc}$ ,  $I_{ph0}$  is the photo-current measured under standard conditions ( $E_{sc}$  and  $T_{sc}$ , where  $E_{sc} = 1,000$  W/m<sup>2</sup> and  $T_{sc} = 25$  °C), and  $J_i$  is the temperature coefficient of the short-circuit current.

**2.3. Modeling of the BOOST DC/DC converter**

To ensure the continuous and efficient operation of the photovoltaic (PV) module at its maximum power point (MPP), a critical component comes into play—a DC/DC converter, as visually represented in Figure 6. This converter plays a pivotal role by facilitating the adjustment of the PV-generated voltage, denoted as  $V_{pv}$ , to align with its designated reference value [34]. The dynamic functionality of this converter becomes particularly crucial in varying environmental conditions, allowing the PV system to adapt seamlessly and consistently harvest the maximum available power from the solar irradiance.

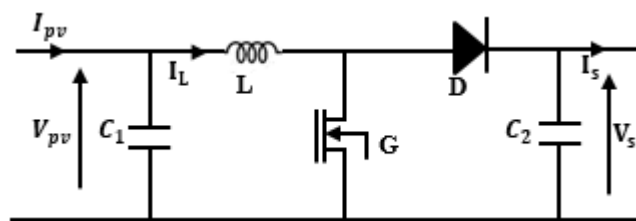


Figure 6. Equivalent circuit of a boost DC/DC converter

Using The averaged model of the entire system is described by the following equations [37], employing Kirchoff's voltage and current laws:

$$\frac{dV_{pv}}{dt} = \frac{1}{C_1} (I_{pv} - I_L) \tag{5a}$$

$$\frac{dI_L}{dt} = \frac{1}{L} V_{pv} - \frac{1}{L} (1 - d)V_{dc} \tag{5b}$$

$$\frac{dV_{dc}}{dt} = \frac{1}{C_2} (I_L(1 - d) - I_s) \tag{5c}$$

Where:  $V_{pv}$  represents the PV output voltage,  $I_L$  is the current flowing through the inductor of the boost converter,  $V_{dc}$  is the DC-link voltage,  $I_s$  is the inverter-side inductor current, and  $d$  is the duty cycle utilized for switching the boost converter by generating the PWM output.

$$\text{Where : } d = \begin{cases} 1 & \text{if } G : ON \\ 0 & \text{if } G : OFF \end{cases}$$

**2.4. Modeling of the three-phase DC/AC inverter**

The PV system is linked to the grid through a three-phase (DC/AC) inverter. This inverter delivers the ultimate current to the grid using six transistors (IGBTs) and anti-parallel diodes. The connection between the DC/AC inverter and the grid involves an LC filter, employed to diminish the ripple components induced by the switching actions of the PWM inverter [38]. The relationship between the three-phase voltages of the DC/AC inverter and the DC bus voltage is expressed as follows:

$$\begin{bmatrix} v_a \\ v_b \\ v_c \end{bmatrix} = \frac{1}{3} \begin{bmatrix} 2 & -1 & -1 \\ -1 & 2 & -1 \\ -1 & -1 & 2 \end{bmatrix} \begin{bmatrix} S_a \\ S_b \\ S_c \end{bmatrix} V_{dc} \tag{6}$$

Where:  $v_a$ ,  $v_b$ , and  $v_c$  represent the inverter output voltages, and  $S_a$ ,  $S_b$ , and  $S_c$  denote the PWM switching signals for the DC/AC inverter.  $v_{dc}$  is the link voltage. The dynamic model of a voltage source inverter with an LC filter is described by the following system of equations [39]:

$$\frac{di_a}{dt} = -\frac{r_f}{L_f}i_a - \frac{1}{L_f}E_{ga} + \frac{v_{dc}}{3L_f}(2S_a - S_b - S_c) \quad (7a)$$

$$\frac{di_b}{dt} = -\frac{r_f}{L_f}i_b - \frac{1}{L_f}E_{gb} + \frac{v_{dc}}{3L_f}(-S_a + 2S_b - S_c) \quad (7b)$$

$$\frac{di_c}{dt} = -\frac{r_f}{L_f}i_c - \frac{1}{L_f}E_{gc} + \frac{v_{dc}}{3L_f}(-S_a - S_b + 2S_c) \quad (7c)$$

Where  $i_a$ ,  $i_b$ , and  $i_c$  represent the inverter currents, and  $E_{ga}$ ,  $E_{gb}$ , and  $E_{gc}$  are the output voltages.  $L_f$  is the inductance of the filter, and  $r_f$  is the line resistance.  $S_a$ ,  $S_b$  and  $S_c$  are signals employed by PWM to generate the switching signals of the inverter  $s_{i=a,b,c}^*$ :

$$\text{Where : } s_{i=a,b,c}^* = \begin{cases} 1 & \text{if } S_i: ON ; S_i': OFF \\ 0 & \text{if } S_i: OFF ; S_i': ON \end{cases}$$

And  $E_{gi(i=a,b,c)} = V_{gi} + V_{la}$  with  $V_{gi}$  are the grid voltages and  $V_{la}$  are the load voltages.

Addressing the challenges of controller design in the (abc) framework, the Park transformation provides a powerful solution: It transforms three-phase quantities into their DC equivalents in the (dq0) frame, significantly reducing complexity. To derive a suitable dynamic model, it is necessary to transform it into an orthogonal synchronous frame rotating at the power system's angular frequency ( $\omega=2\pi f$ ) [26], [40]. When viewed from a frame of reference that rotates in sync with the grid's angular frequency, the mathematical model of the grid-integrated three-phase inverter takes on a specific form, as follows:

$$\frac{di_d}{dt} = -\frac{r_f}{L}i_d + \omega i_q - \frac{1}{L}E_{gd} + \frac{1}{L}v_{dc}S_d \quad (8a)$$

$$\frac{di_q}{dt} = -\frac{r_f}{L}i_q - \omega i_d - \frac{1}{L}E_{gq} + \frac{1}{L}v_{dc}S_q \quad (8b)$$

$$\text{Where : } \begin{bmatrix} i_d \\ i_q \end{bmatrix} = P_{abc}^{dq0} \begin{bmatrix} i_a \\ i_b \\ i_c \end{bmatrix}; \begin{bmatrix} S_d \\ S_q \end{bmatrix} = P_{abc}^{dq0} \begin{bmatrix} S_a \\ S_b \\ S_c \end{bmatrix}; \begin{bmatrix} E_{gd} \\ E_{gq} \end{bmatrix} = P_{abc}^{dq0} \begin{bmatrix} E_{ga} \\ E_{gb} \\ E_{gc} \end{bmatrix}; \omega = \frac{d\theta}{dt}$$

$$P_{abc}^{dq} = \frac{2}{3} \begin{pmatrix} \sin(\theta) & \sin(\theta - \frac{2\pi}{3}) & \sin(\theta + \frac{2\pi}{3}) \\ \cos(\theta) & \cos(\theta - \frac{2\pi}{3}) & \cos(\theta + \frac{2\pi}{3}) \\ \frac{1}{2} & \frac{1}{2} & \frac{1}{2} \end{pmatrix}$$

Where  $[E_{gd}, E_{gq}]$ ,  $[i_d, i_q]$  and  $[S_d, S_q]$  represent, respectively, the output voltages, injected currents, and the PWM input components in the d-q axis. It is essential to employ a phase-locked loop (PLL) to synchronize pulse width modulation (PWM) and the DC/AC inverter control with the grid voltage, determining the network's phase angle [41], represented by  $\theta$ . The active and reactive power of a three-phase system can be expressed as:

$$P = \frac{3}{2}(E_{gd}i_d + E_{gq}i_q) \quad (9a)$$

$$Q = \frac{3}{2}(E_{gq}i_d - E_{gd}i_q) \quad (9b)$$

At steady-state, the average value of  $E_{gq}$  in a synchronously rotating (dq0) reference frame can be considered to be zero. Consequently, in (9a)–(9b) can be simplified as follows:

$$P = \frac{3}{2}E_{gd}i_d \quad (10a)$$

$$Q = -\frac{3}{2} E_{gd} i_q \tag{10b}$$

Assuming the DC/AC inverter is lossless, the power on the AC and DC sides must be equal, expressed as follows:

$$v_{dc} I_s = \frac{3}{2} E_{gd} i_d \tag{11}$$

$$I_s = \frac{3}{2v_{dc}} E_{gd} i_d \tag{12}$$

The DC link voltage presented in (5c) can be rewritten in (13):

$$\frac{dv_{dc}}{dt} = \frac{1}{C_2} (I_L(1 - d) - \frac{3}{2v_{dc}} E_{gd} i_d) \tag{13}$$

The d and q-axis currents influence the active and reactive power injected into the network. Consequently, the control of this power depends on the injected currents  $i_d$  and  $i_q$ .

### 3. PROPOSED CONTROLLER DESIGN

This section focuses on the design of nonlinear controllers to fulfill all objectives of the PV system connected to the three-phase grid. Figure 7 provides an overview of each controller. The first controller is associated with the PV voltage, ensuring PSO monitoring of the maximum power point (MPPT) and implementing backstepping regulation for the voltage supplied by the PV generator. The second controller comprises two loops: the internal loop ensures achievement of the UPF objective, while the external loop is designed to regulate the output voltage of the DC link capacitor.

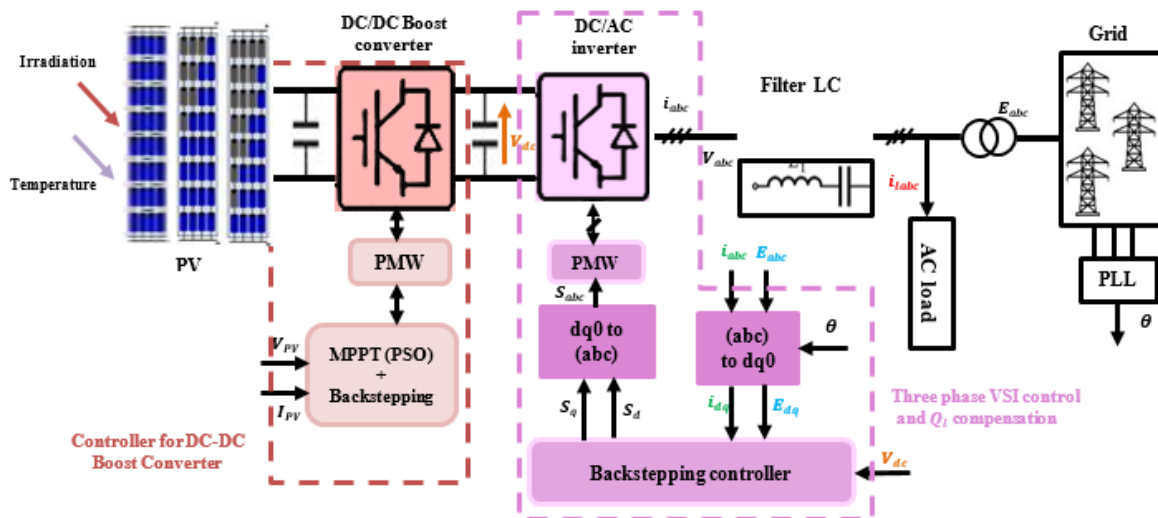


Figure 7. Block diagram of the nonlinear control scheme of the three-phase-grid connected PV system feeding AC load

#### 3.1. MPPT controller design

When the PV panel is exposed to PSC, extracting the maximum power becomes challenging due to the nonlinearity of the power-voltage (P-V) curve, which exhibits multiple local peaks. Overcoming this challenge requires the use of evolutionary algorithms (EA), among which PSO is employed. In this method, each particle involved in the process is fully characterized in terms of position  $x_i$  and velocity  $v_i$ , as indicated by (14) and (15). Each particle suggests a solution by exchanging data gathered in its search process to identify the optimal answer [42], [43]. The particles utilize two final values, best individual position  $P_{best}$  and best group position  $G_{best}$ , to update their positions and velocities. Figure 8 illustrates the flowchart of the PSO method.

$$x_i^{k+1} = x_i^k + v_i^{k+1} \quad (14)$$

$$v_i^{k+1} = wv_i^k + m_1r_1(P_{best} - x_i^k) + m_2r_2(G_{best} - x_i^k) \quad (15)$$

In this study, the output voltage of the PV cell serves as the parameter guiding the swarm particles towards the MPP. The reference voltage,  $V_{ref}$ , and the output power of the PV system are determined by the position and velocity of the particle swarm [42], [44]. Consequently, (14) can be modified and expressed as (16).

$$V_{ref-i}^{k+1} = V_{ref-i}^k + P_{s,i}^{k+1} \quad (16)$$

The parameters used are: the size of population 5, inertia weight  $w = 0.4$ , acceleration coefficients  $m_1 = 1.2$  and  $m_2 = 1$ , random variables  $r_1$  and  $r_2 = 0.5$ . When solar irradiation is detected, the initial population is reset, as described:

$$|V_{pv}(k+1) - V_{pv}(k)| = \Delta V_{pv} \quad (17)$$

$$\left| \frac{P_{pv}(k+1) - P_{pv}(k)}{P_{pv}(k)} \right| = \Delta P \quad (18)$$

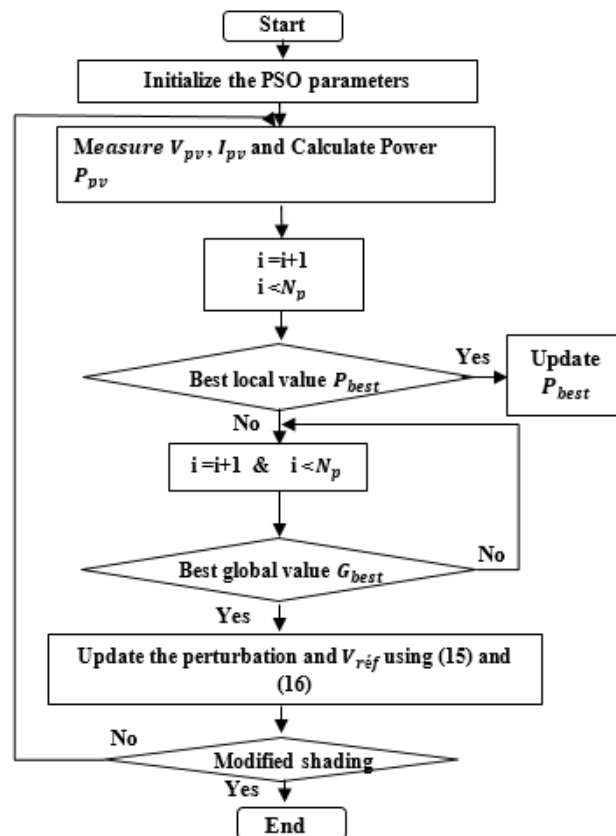


Figure 8. Flowchart of the PSO algorithm

### 3.2. Design of an adaptive controller for the DC-DC boost converter

To achieve optimal power extraction and grid integration, the backstepping controller works hand-in-hand with the PSO algorithm. It meticulously adjusts the PV output voltage to match the PSO-determined reference value,  $V_{ref}$ , ensuring MPP tracking and efficient energy transfer to the grid. This objective is achieved by modifying the duty cycle of a DC-DC boost converter to extract the maximum power under various weather conditions [9]. The controller is designed in two steps:

Step 1: In the initial stage, we determine the reference voltage,  $V_{ref}$ , followed by  $V_{pv}$ . We define the tracking error as follows:

$$e_1 = V_{pv} - V_{ref} \tag{19}$$

The derivative with time respect to  $e_1$  is given by:

$$\dot{e}_1 = \dot{V}_{pv} - \dot{V}_{ref} = \frac{1}{C_1}(I_{pv} - I_L) - \dot{V}_{ref} \tag{20}$$

We consider the first Lyapunov candidate function to ensure stability:

$$V_1 = \frac{1}{2} e_1^2 \tag{21}$$

The time derivative of  $V_1$  is given by:

$$\dot{V}_1 = e_1 \dot{e}_1 = e_1 \left( \frac{I_{pv} - I_L}{C_1} - \dot{V}_{ref} \right) \tag{22}$$

In (22) must be negative. Or,  $\dot{V}_1(e_1)$  can also be expressed as follows:

$$\dot{e}_1 = -K_1 e_1, \dot{V}_1(e_1) = -K_1 e_1^2 \leq 0 \tag{23}$$

With  $K_1$  is a positive constant ( $K_1 > 0$ ) which represents a design parameter of the backstepping controller.

$$e_1 \left( \frac{I_{pv} - I_L}{C_1} - \dot{V}_{ref} \right) = -K_1 e_1^2 \tag{24}$$

Let's introduce a placeholder variable,  $\alpha = I_L$  to act as a virtual control. It mirrors the desired value for the state variable,  $I_L$ . Now, let's explore how  $\alpha$  changes over time by examining its time derivative:

$$\alpha = I_{pv} - C_1 \dot{V}_{ref} + K_1 C_1 e_1 \tag{25}$$

Its derivative is:

$$\dot{\alpha} = \dot{I}_{pv} - C_1 \ddot{V}_{ref} + K_1 C_1 \dot{e}_1 \tag{26}$$

Step 2: To ensure the state variable closely aligns with its intended value, we introduce a second tracking error in this step. This error serves as a guide for control strategies aimed at minimizing it:

$$e_2 = I_L - \alpha, \dot{e}_2 = \dot{I}_L - \dot{\alpha} = \frac{1}{L}(V_{pv} - (1-d)V_s) - \dot{\alpha} \tag{27}$$

The second Lyapunov function of the system to be controlled, in the state space  $V_2(e_1, e_2)$  are written:

$$V_2 = V_1 + \frac{1}{2} e_2^2, \dot{V}_2 = \dot{V}_1(e_1) + e_2 \dot{e}_2 \tag{28}$$

The new expression of the time derivative of the Lyapunov function  $V_1$  a be obtained:

$$\dot{V}_1 = -K_1 e_1^2 - \frac{e_1 e_2}{C_1} \tag{29}$$

The time derivative of  $V_2(e_1, e_2)$  becomes as follows:

$$\dot{V}_2 = -K_1 e_1^2 + e_2 \dot{e}_2 - \frac{e_1 e_2}{C_1} \tag{30a}$$

$$\dot{V}_2 = -K_1 e_1^2 + e_2 \left( \dot{I}_L - \dot{\alpha} - \frac{e_1}{C_1} \right) \tag{30b}$$

$$\dot{V}_2 = -K_1 e_1^2 + e_2 \left( -\frac{1}{C_1} e_1 + \frac{1}{L}(V_{pv} - (1-d)V_s - \dot{\alpha}) \right) \tag{30c}$$

To ensure that the time derivative of the Lyapunov function  $V_2(e_1, e_2)$  is negative, the previous expression must validate:

$$\left(-\frac{1}{c_1}e_1 + \frac{1}{L}(V_{pv} - (1-d)V_s - \dot{\alpha})\right) = -K_2e_2 \leq 0 \quad (31)$$

With:  $K_2$  is a positive design parameter. Combining (30c) and (31), the final control law  $d$  is obtained:

$$d = 1 - \frac{1}{V_s} \left[ V_{pv} - L\alpha - L \left( \frac{1}{c_1}e_1 - K_2e_2 \right) \right] \quad (32)$$

The second Lyapunov function of the system:

$$\dot{V}_2(e_1, e_2) = -K_1e_1^2 - K_2e_2^2 \quad (33)$$

The control law derived from this expression guarantees that the errors ( $e_1$ ) and ( $e_2$ ) eventually diminish to zero, effectively steering the system's state variables towards their desired values  $V_{pv}$  at the origin  $V_{ref}$ .

### 3.3. Backstepping controller for three-phase DC/AC

The nonlinear backstepping controller is applied in this section to generate switching control inputs for the DC/AC inverter, aiming to achieve the desired tracking of all states in the dynamic model of the grid-connected PV system. Subsequent paragraphs will elaborate on the detailed design steps.

Step 1: controlling the  $V_{dc}$  link voltage is crucial to ensure the proper operation and reliability of the grid-connected PV system, guaranteeing optimal energy production and a stable power supply for grid users. The monitoring of  $V_{dc}$  involves analyzing it with consideration for  $V_{dc}^*$  as its desired value. The tracking error between the actual and desired values of the voltage  $V_{dc}$  is expressed as follows:

$$e_3 = V_{dc} - V_{dc}^* \quad (34)$$

The time derivative of the tracking error  $e_3$  as using (11):

$$\dot{e}_3 = \dot{V}_{dc} - \dot{V}_{dc}^* = \frac{1}{c_2}(I_L(1-d) - \frac{3}{2v_{dc}}E_{gd}i_d) - \dot{V}_{dc}^* \quad (35)$$

As  $V_{dc}^*$  is a constant its derivative is null  $\dot{V}_{dc}^* = 0$ . The Lyapunov candidate function (LCF) and its derivative are used to demonstrate stability as follows:

$$V_3 = \frac{1}{2}e_3^2, \dot{V}_3 = e_3\dot{e}_3 = e_3 \left[ \frac{1}{c_2}(I_L(1-d) - \frac{3}{2v_{dc}}E_{gd}i_d) \right] \quad (36)$$

To stabilize the tracking error  $e_3$  at zero,  $\dot{V}_3$  must be a negative semidefinite function ( $\dot{V}_3 < 0$ ). To do this, the state variable  $i_d$  acts as a virtual control:

$$i_d^* = \alpha_1 = \frac{2c_2V_{dc}}{3E_{gd}} \left[ K_3e_3 + \frac{I_L(1-d)}{c_2} \right] \quad (37)$$

The virtual control  $i_d^*$  ensures that the (37) results in negative semi-definite function  $\dot{V}_3 = -K_3e_3^2$

Step 2:  $\alpha_1$  does not represent the actual control input  $i_d$ ; there exists an error between the two. The subsequent step is designed to yield direct and quadratic current components  $i_d$  and  $i_q$  that are sinusoidal and in phase with the grid supply voltage, thereby achieving a UPF. Assuming no energy loss at the inverter (though there is some), the maximum amount of active power that can be fed into the grid is denoted as  $P_{max}$ . Additionally,  $P_{max}$  must align with the active power  $P$ . To inject the maximum active power and minimize reactive power, this internal current regulation loop ensures that current values  $i_d$  and  $i_q$  align with the specified reference values.

To attain this objective, it is essential to define the tracking error as follows:

$$e_4 = i_d - \alpha_1, \dot{e}_4 = \dot{i}_d - \dot{\alpha}_1 = -\frac{r_f}{L}i_d + \omega i_q - \frac{1}{L}E_{gd} + \frac{1}{L}v_{dc}S_d - \dot{\alpha}_1 \quad (38)$$

On the other hand, we defined the q-axis current tracking error  $i_q$  in (39) with  $\alpha_2 = i_q^*$ :

$$e_5 = i_q - \alpha_2, \dot{e}_5 = \dot{i}_q - \dot{\alpha}_2 = -\frac{r_f}{L}i_q + \omega i_d - \frac{1}{L}E_{gq} + \frac{1}{L}v_{dc}S_q - \dot{\alpha}_2 \tag{39}$$

We can obtain the control input signals  $S_d$  and  $S_q$ , by defining an augmented Lyapunov candidate function (LCF):

$$W = V_1 + V_2 + V_3 + \frac{1}{2}e_4^2 + \frac{1}{2}e_5^2 \tag{40}$$

Its derivative can be written as follows:

$$\dot{W} = \dot{V}_1 + \dot{V}_2 + \dot{V}_3 + \dot{e}_4e_4 + \dot{e}_5e_5 \tag{41}$$

By replacing the values of  $\dot{V}_3, \dot{e}_4$  and  $\dot{e}_5$  in (41), we obtain:

$$\begin{aligned} \dot{W} = & -K_1e_1^2 - K_2e_2^2 - K_3e_3^2 + e_4 \left[ -\frac{r_f}{L}i_d + \omega i_q - \frac{1}{L}E_{gd} + \frac{1}{L}v_{dc}S_d - \dot{\alpha}_1 \right] \\ & + e_5 \left[ -\frac{r_f}{L}i_q + \omega i_d - \frac{1}{L}E_{gq} + \frac{1}{L}v_{dc}S_q - \dot{\alpha}_2 \right] \end{aligned} \tag{42}$$

$\dot{W} < 0$  to ensure error stability of the subsystem. At last, the stabilizing switching control laws can be expressed as:

$$S_d = \frac{L}{v_{dc}} \left[ \frac{r_f}{L}i_d - \omega i_q + \dot{\alpha}_1 - K_4e_4 + \frac{E_{gd}}{L} \right] \tag{43a}$$

$$S_q = \frac{L}{v_{dc}} \left[ \frac{r_f}{L}i_q - \omega i_d + \dot{\alpha}_2 - K_5e_5 + \frac{E_{gq}}{L} \right] \tag{43b}$$

where:  $K_4$  and  $K_5$  are the positive parameters and according to (43a) and (43b):

$$\dot{W} = -K_1e_1^2 - K_2e_2^2 - K_3e_3^2 - K_4e_4^2 - K_5e_5^2 \leq 0 \tag{44}$$

Finally, the proposed backstepping control successfully accomplishes all the defined objectives, ensuring the global asymptotic stability of the entire system. The application of the backstepping control is effective in meeting the specified goals and maintaining the overall stability of the system on a global scale.

#### 4. SIMULATION AND ANALYSIS OF RESULTS

The configuration under examination in this study comprises six groups. In each group, there are three panels connected in series and 28 in parallel. The SunPower SPR-400E-WHT-D module was chosen to assess the performance of the proposed system under PSC, as discussed in section 2. Table 1 presents the specifications for the PV modules, the BOOST converter, and the grid parameters.

Table 1. The SPR-400E-WHT-D PV module, boost and grid parameter

Parameters	Nomenclature	Values
Voltage at open cct	$V_{oc}$	85,3 V
Short cct-current	$I_{sc}$	5,87 A
Max power voltage	$V_{mpp}$	72,9 V
Max power current	$I_{mpp}$	5,49 A
Photo-current	$I_{ph}$	5,8772 A
Saturation current	$I_0$	$6,9161e^{-13}$ A
Diode ideality	A	0,87221
Series resistance	$R_s$	0,5572 $\Omega$
Input capacitor	$C_1$	220e-5 F
Output capacitance	$C_2$	1000e-3 F
Inductance	L	0.67e-3H
Frequency	S	10 KHz
DC Link voltage	$V_{dc}$	800 V
Grid (V/f)	$V_g/f$	380V/50Hz
Boost backstepping controller	$K_1$	1000e-3
	$K_2$	1/0.67e-3
Inverter backstepping controller	$K_3$	1/700
	$K_4$	314.16
	$K_5$	1963.5

We opted to evaluate the controller's performance under PSC, as depicted in Figure 9. This assessment was carried out with a deliberate effort to maintain a constant temperature of 25 °C. This choice aimed to ensure a controlled and consistent thermal environment throughout the testing process:

- Group 1 and 2: 1,000 W/m<sup>2</sup> during the whole simulation time [0 to 1.5].
- Group 3 and 4: 1,000 W/m<sup>2</sup> during [0 to 0.5] and 800 W/m<sup>2</sup> during [0.5 to 1.5].
- Group 5 and 6: 1,000 W/m<sup>2</sup> during [0 to 1] and 500 W/m<sup>2</sup> during [1 to 1.5].

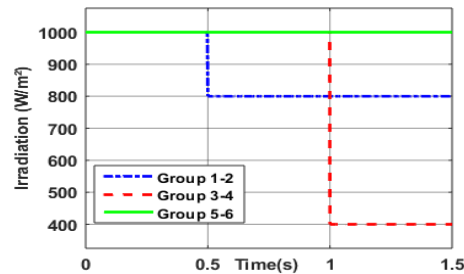


Figure 9. Irradiance profile under partial shading condition

It is essential to highlight that, based on the literature, the radiation level remains relatively constant within time intervals of less than 5 or 6 seconds. In an effort to reduce simulation time, we have decided to decrease the intervals for radiation changes from 5 seconds to 1.5 seconds in this paper. Figure 10 illustrates the control performance of the PV system under solar irradiation variations. The depicted graphs demonstrate that the PV system controller, which integrates the PSO algorithm and the backstepping controller, effectively tracks the MPP of solar energy, even in the presence of partial shading.

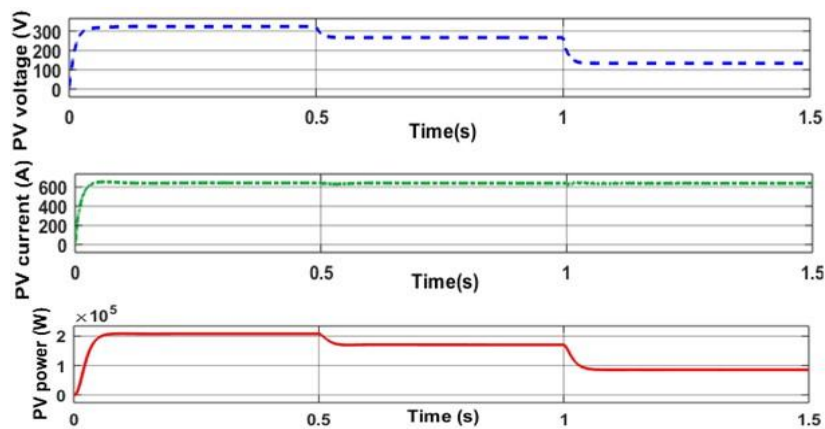


Figure 10. The control performance assessment of PV systems

The parameters generated by the PV panel exhibit variations not only in response to changes in radiation intensity but also based on the dynamic characteristics of the AC load connected to the system output. The intricate interplay between these factors underscores the need for robust control strategies. To rigorously evaluate the effectiveness of the proposed control methodologies, comprehensive MATLAB/Simulink simulations were meticulously conducted. The obtained results are thoroughly scrutinized, providing valuable insights into the system's behavior under varying conditions. The assessment encompasses three specific scenarios, as delineated in Figure 11, allowing a nuanced understanding of the control strategies' performance across diverse operational contexts.

Scenario 1: The PV power is higher than the power required by the AC load ( $P_{pv} > P_{load}$ )

The case study for this scenario is conducted within the interval [0 - 0.5], during which the six PV groups are exposed to a uniform initial irradiation level of 1,000 W/m<sup>2</sup>. In this instance, the PV system

generates a maximum power of 208 kW, fulfilling the AC load demand of 100 kW, and the surplus power (100 kW) is supplied to the grid.

Scenario 2: The power demanded by the AC load is greater than the PV power ( $P_{pv} < P_{load}$ )

A sudden shadow affecting PV groups 3 and 4 leads to a reduction in irradiation levels to 800 W/m<sup>2</sup>. Consequently, the maximum power generated by the PV system in this scenario reaches 170.5 kW, falling below the demand from the AC load (204 kW). To address this shortfall, the grid supplements the load demand by providing 34 kW of power.

Scenario 3: No demand of the AC load  $P_{load} = 0$  kW

In this particular case, the load demand is zero, and the irradiation, at 400 W/m<sup>2</sup>, has changed due to partial shading impacting groups 5 and 6. Consequently, the maximum power output from the PV system amounts to 85 kW, which is then sold to the grid.

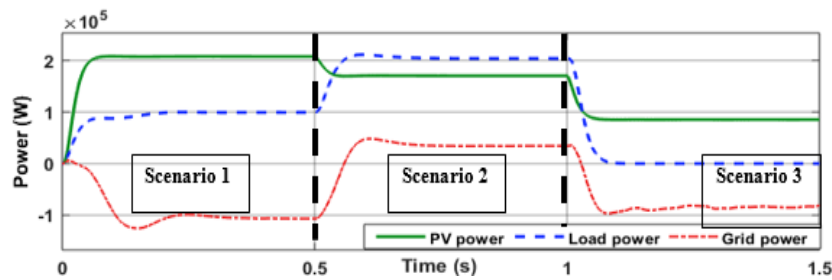


Figure 11. Power profiles of solar PV array, AC load, and grid under different operating conditions

The graph in Figure 12 underscores the backstepping control's proficiency in ensuring DC bus voltage stability and responsiveness.  $V_{dc}$  resolutely adheres to its 800 V target despite power variations, and it swiftly recovers after irradiation changes occur at 0.5 and 1 second. These findings highlight the control strategy's ability to maintain a consistent and dependable voltage output.

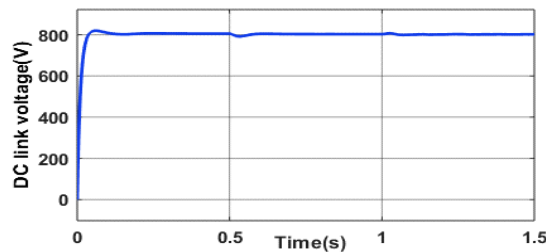


Figure 12. Dynamic profile of DC link voltage

The simulation results paint a clear picture of the Backstepping control's effectiveness. Observe how the grid current of phase (a) gracefully aligns with the corresponding grid voltage as shown in Figure 13, forming a perfect sinusoidal partnership. This harmonious relationship extends to phases (b) and (c), showcasing the control's ability to deliver power efficiently while maintaining a UPF.

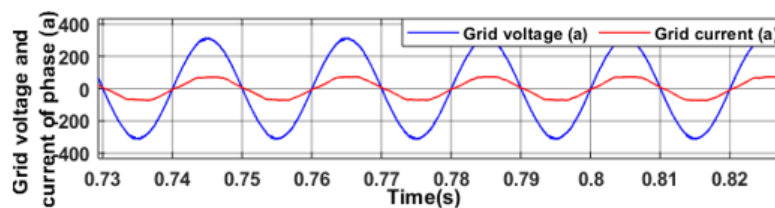


Figure 13. The current and voltage injected into one phase of the network (phase a)

In summary, the study explores the impact of varying conditions on PV panel parameters, including changes in radiation intensity and AC load demand. To assess the effectiveness of proposed control strategies in three specific scenarios, shedding light on the system's behavior and its interaction with the grid under different circumstances. Backstepping control has been shown to be effective in maintaining the stability of the DC bus voltage (Vdc) and managing power variations. It has demonstrated a rapid and accurate convergence capability independently of irradiation and AC load changes. In addition, backstepping control has ensured a sinusoidal and in-phase grid current with the corresponding grid voltage for the same phase, while maintaining a unit power factor. These results underline the reliability and robustness of backstepping control in managing grid-connected PV systems, even in the presence of abrupt parameter variations.

## 5. CONCLUSION

In our paper, we propose a nonlinear control approach for a three-phase grid-connected PV system supplying an AC load and connected to an LC filter. The simulation results of our system have demonstrated its significance and effectiveness in various operational scenarios, including PSC. Specifically, we have shown that all our control objectives are achieved, with improved results compared to other methods. Looking ahead, our future research will focus on a nonlinear control strategy for a grid-connected PV-wind hybrid system. Considering PSC, this strategy will be designed to efficiently extract energy from both sources while meeting grid interconnection requirements. The utilization of our nonlinear backstepping controller is expected to enhance the robustness and performance of the hybrid system, making a substantial contribution to the field of renewable energy.

## REFERENCES

- [1] H. U Rehman, X. Yan, M. A. Abdelbaky, M. Ullah Jan, and S. Iqbal, "An advanced virtual synchronous generator control technique for frequency regulation of grid-connected PV system," *Int. J. Electr. Power Energy Syst.*, vol. 125, no. August 2020, p. 106440, 2021, doi: 10.1016/j.ijepes.2020.106440.
- [2] B. Mbarki, F. Farhani, and A. Zaafouri, "Comparative study of some Maximum Power Point Tracking algorithms," *Conference Record of the Twenty-Eighth IEEE Photovoltaic Specialists Conference - 2000 (Cat. No.00CH37036)*, pp. 145–149, 2019, doi: 10.1109/SCC47175.2019.9116145.
- [3] A. D. G. Jegha, M. S. P. Subathra, N. M. Kumar, U. Subramaniam, and S. Padmanaban, "A high gain DC-DC converter with grey wolf optimizer based MPPT algorithm for PV fed BLDC motor drive," *Appl. Sci.*, vol. 10, no. 8, 2020, doi: 10.3390/AP10082797.
- [4] H. Yatimi and E. Aroudam, "Assessment and control of a photovoltaic energy storage system based on the robust sliding mode MPPT controller," *Sol. Energy*, vol. 139, pp. 557–568, 2016, doi: 10.1016/j.solener.2016.10.038.
- [5] S. Khadija, E. M. Ouadia, and F. Abdelmajid, "Tracking the GMPP of a solar photovoltaic water pumping system with an SMC controller in partial shading conditions," *Bulletin of Electrical Engineering and Informatics*, vol. 12, no. 6, pp. 3298–3310, 2023, doi: 10.11591/eei.v12i6.5504.
- [6] V. K. Arun Shankar, S. Umashankar, S. Padmanaban, M. S. Bhaskar, V. K. Ramachandaramurthy, and V. Fedák, "Comparative study of photovoltaic based power converter topologies for pumping applications," *2017 IEEE Conference on Energy Conversion (CENCON)*, vol. 2018-Janua, pp. 174–179, 2017, doi: 10.1109/CENCON.2017.8262479.
- [7] P. Talebi and M. Hejri, "Distributed Control of a Grid-connected PV-battery System for Constant Power Generation," *Journal of Energy Management and Technology (JEMT)*, vol. 3, no. 3, pp. 14–29, 2019.
- [8] F. K. Abo-Elyousr and A. Y. Abdelaziz, "Optimal PI microcontroller-based realization for technical trends of single-stage single-phase grid-tied PV," *Engineering Science and Technology, an International Journal*, vol. 21, no. 5, pp. 945–956, 2018, doi: 10.1016/j.jestch.2018.07.007.
- [9] R. A. Soumana, M. J. Saulo, and C. M. Muriithi, "New control strategy for multifunctional grid-connected photovoltaic systems," *Results Eng.*, vol. 14, no. April, p. 100422, 2022, doi: 10.1016/j.rineng.2022.100422.
- [10] X. Yan, C. Wang, Z. Wang, H. Ma, B. Liang, and X. Wei, "A united control strategy of photovoltaic-battery energy storage system based on voltage-frequency controlled vsq," *Electronics*, vol. 10, no. 17, pp. 1–17, 2021, doi: 10.3390/electronics10172047.
- [11] S. Marhraoui, A. Abbou, Z. Cabrane, S. E. Rhaili, and N. El Hichami, "Fuzzy logic-integral backstepping control for PV grid-connected system with energy storage management," *Int. J. Intell. Eng. Syst.*, vol. 13, no. 3, pp. 359–372, 2020, doi: 10.22266/IJIES2020.0630.33.
- [12] Z. Yi, W. Dong, and A. H. Etemadi, "A unified control and power management scheme for PV-Battery-based hybrid microgrids for both grid-connected and islanded modes," *IEEE Trans. Smart Grid*, vol. 9, no. 6, pp. 5975–5985, 2018, doi: 10.1109/TSG.2017.2700332.
- [13] A. Abouloifa, C. Aouadi, I. Lachkar, Y. Boussairi, M. Aourir, and A. Hamdoun, "Output-Feedback Nonlinear Adaptive Control Strategy of the Single-Phase Grid-Connected Photovoltaic System," *J. Sol. Energy*, vol. 2018, pp. 1–14, 2018, doi: 10.1155/2018/6791056.
- [14] O. E. L. Maguiri and A. Farchi, "Nonlinear controller design for maximum power tracking in grid connected photovoltaic systems . 2 Presentation and Modeling of Grid connected PV system .," vol. 10, pp. 513–519, 2015.
- [15] K. Sabri, O. El Maguiri, and A. Farchi, "Comparative Study of Different MPPT Algorithms for Photovoltaic Systems under Partial Shading Conditions," *Proc. 2021 9th Int. Renew. Sustain. Energy Conf. IRSEC 2021*, 2021, doi: 10.1109/IRSEC53969.2021.9741164.

- [16] S. Akram, L. Khalil, M. K. L. Bhatti, T. Aftab, R. Siddique, and M. Riaz, "Maximum Power Point Tracking using Direct Control with Cuckoo Search for Photovoltaic Module under Partial Shading Condition," *Pakistan Journal of Engineering and Technology*, vol. 4, no. 2, pp. 28–31, 2021, doi: 10.51846/vol4iss2pp28-31.
- [17] F. K. Abo-Elyousr, A. M. Abdelshafy, and A. Y. Abdelaziz, "MPPT-based particle swarm and cuckoo search algorithms for PV systems," *Green Energy Technol.*, pp. 379–400, 2020, doi: 10.1007/978-3-030-05578-3\_14.
- [18] P. K. B. Mallappa, H. Martínez-García, and G. Velasco-Quesada, "Power quality improvements in grid-connected PV system using hybrid technology," *Renew. Energy Power Qual. J.*, vol. 19, no. 19, pp. 316–320, 2021, doi: 10.24084/repqj19.284.
- [19] A. D. Martin, J. R. Vazquez, and R. S. Herrera, "Adaptive backstepping control of a DC-DC converter in photovoltaic systems," *IEEE EuroCon 2013*, no. July, pp. 949–955, 2013, doi: 10.1109/EUROCON.2013.6625096.
- [20] A. Saxena, H. M. Suryawanshi, A. B. Shitole, G. G. Talapur, and A. A. Chanekar, "Energy management of photovoltaic and battery energy storage based grid tied three level inverter system," *2017 7th Int. Conf. Power Syst. ICPS 2017*, pp. 139–144, 2018, doi: 10.1109/ICPES.2017.8387282.
- [21] P. R. Rivera, M. L. McIntyre, M. Mohebbi, and J. Latham, "Single - Stage three - Phase grid - Connected photovoltaic system with maximum power tracking and active and reactive power control based on nonlinear control," *2017 IEEE Energy Convers. Congr. Expo. ECCE 2017*, vol. 2017-Janua, pp. 1–7, 2017, doi: 10.1109/ECCE.2017.8095753.
- [22] A. El Fadili *et al.*, "Backstepping Control of Photovoltaic-Grid Hybrid Power Feed Water Pump," *IFAC-PapersOnLine*, vol. 50, no. 1, pp. 6540–6545, 2017, doi: 10.1016/j.ifacol.2017.08.601.
- [23] M. H. Boujmil, A. Badis, and M. Nejib Mansouri, "Nonlinear Robust Backstepping Control for Three-Phase Grid-Connected PV Systems," *Math. Probl. Eng.*, vol. 2018, 2018, doi: 10.1155/2018/3824628.
- [24] B. BOUMEDIENE, "Backstepping Control Strategy for Multi-source Energy System based Flying capacitor Inverter and PMSG," *Przeegląd Elektrotechniczny*, vol. 1, no. 3, pp. 23–31, 2021, doi: 10.15199/48.2021.03.04.
- [25] T. K. Roy and M. A. Mahmud, "Dynamic Stability Analysis of Hybrid Islanded DC Microgrids Using a Nonlinear Backstepping Approach," *IEEE Syst. J.*, vol. 12, no. 4, pp. 3120–3130, 2018, doi: 10.1109/JSYST.2017.2769692.
- [26] T. K. Roy, M. A. Mahmud, S. N. Islam, N. Rajasekar, K. M. Muttaqi, and A. M. T. Oo, "Nonlinear Backstepping Controller Design for Grid-Connected Photovoltaic Systems with Output LC Filters to Improve Dynamic Stability and Power Quality," *2020 IEEE Int. Conf. Power Electron. Smart Grid Renew. Energy, PESGRE 2020*, pp. 1–5, 2020, doi: 10.1109/PESGRE45664.2020.9070616.
- [27] H. Abouobaida, "Robust and efficient controller to design a standalone source supplied DC and AC load powered by photovoltaic generator," *Am. J. Eng. Appl. Sci.*, vol. 9, no. 4, pp. 894–901, 2016, doi: 10.3844/ajeassp.2016.894.901.
- [28] S. Xie, X. Wang, C. Qu, X. Wang, and J. Guo, "Impacts of different wind speed simulation methods on conditional reliability indices," *Int. Trans. Electr. energy Syst.*, vol. 20, pp. 1–6, 2013, doi: 10.1002/etep.
- [29] B. Karanayil, V. G. Agelidis, and J. Pou, "Evaluation of DC-link decoupling using electrolytic or polypropylene film capacitors in three-phase grid-connected photovoltaic inverters," *IECON Proc. (Industrial Electron. Conf.)*, no. 1, pp. 6980–6986, 2013, doi: 10.1109/IECON.2013.6700290.
- [30] I. Aboudrar, S. El Hani, M. S. Heyine, and N. Naseri, "Dynamic Modeling and Robust Control by ADRC of Grid-Connected Hybrid PV-Wind Energy Conversion System," *Math. Probl. Eng.*, vol. 2019, 2019, doi: 10.1155/2019/8362921.
- [31] A. Mohapatra, B. Nayak, P. Das, and K. B. Mohanty, "A review on MPPT techniques of PV system under partial shading condition," *Renew. Sustain. Energy Rev.*, vol. 80, no. June, pp. 854–867, 2017, doi: 10.1016/j.rser.2017.05.083.
- [32] W. Li, G. Zhang, T. Pan, Z. Zhang, Y. Geng, and J. Wang, "A Lipschitz Optimization-Based MPPT Algorithm for Photovoltaic System under Partial Shading Condition," *IEEE Access*, vol. 7, pp. 126323–126333, 2019, doi: 10.1109/ACCESS.2019.2939095.
- [33] A. Dolara, F. Grimaccia, M. Mussetta, E. Ogliari, and S. Leva, "An evolutionary-based MPPT algorithm for photovoltaic systems under dynamic partial shading," *Appl. Sci.*, vol. 8, no. 4, 2018, doi: 10.3390/app8040558.
- [34] S. Khadija, E. M. Ouadia, and F. Abdelmajid, "Nonlinear backstepping control of a partially shaded photovoltaic storage system," *2019, no. 1, pp. 225–237, 2023*, doi: 10.11591/ijeecs.v29i1.pp225-237.
- [35] M. Jiang, M. Ghahremani, S. Dadfar, H. Chi, Y. N. Abdallah, and N. Furukawa, "A novel combinatorial hybrid SFL–PS algorithm based neural network with perturb and observe for the MPPT controller of a hybrid PV-storage system," *Control Eng. Pract.*, vol. 114, no. June, p. 104880, 2021, doi: 10.1016/j.conengprac.2021.104880.
- [36] R. Kerid and Y. Bounnah, "Modeling and parameter estimation of solar photovoltaic based MPPT control using EKF to maximize efficiency," *Bull. Electr. Eng. Informatics*, vol. 11, no. 5, pp. 2491–2499, 2022, doi: 10.11591/eei.v11i5.3782.
- [37] S. Fahad, A. J. Mahdi, W. H. Tang, K. Huang, and Y. Liu, "Particle Swarm Optimization Based DC-Link Voltage Control for Two Stage Grid Connected PV Inverter," *2018 Int. Conf. Power Syst. Technol. POWERCON 2018 - Proc.*, no. 201807100000006, pp. 2233–2241, 2019, doi: 10.1109/POWERCON.2018.8602128.
- [38] S. Zouga, M. Benchagra, and A. Abdallah, "Backstepping Control Based on the PSO Algorithm for a Three-Phase PV System Connected to the Grid under Load Variation," *2020 Int. Conf. Electr. Inf. Technol. ICEIT 2020*, pp. 0–5, 2020, doi: 10.1109/ICEIT48248.2020.9113235.
- [39] I. S. Kim, "Robust maximum power point tracker using sliding mode controller for the three-phase grid-connected photovoltaic system," *Sol. Energy*, vol. 81, no. 3, pp. 405–414, 2007, doi: 10.1016/j.solener.2006.04.005.
- [40] T. K. Roy, M. A. Mahmud, A. M. T. Oo, R. Bansal, and M. E. Haque, "Nonlinear Adaptive Backstepping Controller Design for Three-Phase Grid-Connected Solar Photovoltaic Systems," *Electr. Power Components Syst.*, vol. 45, no. 20, pp. 2275–2292, 2017, doi: 10.1080/15325008.2018.1431334.
- [41] E. Radwan, K. Salih, E. Awada, and M. Nour, "Modified phase locked loop for grid connected single phase inverter," *Int. J. Electr. Comput. Eng.*, vol. 9, no. 5, pp. 3934–3943, 2019, doi: 10.11591/ijece.v9i5.pp3934-3943.
- [42] J. Farzaneh, R. Keypour, and M. A. Khanesar, "A New Maximum Power Point Tracking Based on Modified Firefly Algorithm for PV System Under Partial Shading Conditions," *Technol. Econ. Smart Grids Sustain. Energy*, vol. 3, no. 1, 2018, doi: 10.1007/s40866-018-0048-7.
- [43] H. Chaieb and A. Sakly, "Comparison between P & O and P . S . O Methods Based MPPT Algorithm for Photovoltaic Systems," pp. 694–699, 2015, doi: 978-1-4673-9234-1/15/\$31.00 ©2015 IEEE.
- [44] K. K. Jha and M. N. Anwar, "Solar Photovoltaic based Brushless DC Motor Driven Water Pumping System using PSO-MPPT Algorithm," *2019 54th Int. Univ. Power Eng. Conf. UPEC 2019 - Proc.*, pp. 1–6, 2019, doi: 10.1109/UPEC.2019.8893591.

**BIOGRAPHIES OF AUTHORS**

**Sabri Khadija**    was born in 1990. He obtained the master's degree in Automatic, Signal Processing, Industrial Computing from Hassan first University, Settat, Morocco, in 2014. He is currently a Ph.D. student at the Research Laboratory in Engineering, Industrial Management and Innovation, Faculty of Science & Technology, Hassan first University. His research interests include monitoring the maximum power of photovoltaic (PV) systems in general, storage systems and pumped-storage systems, partially shaded. The injection of energy into the grid. She can be contacted at email: k.sabri@uhp.ac.ma.



**El Maguiri Ouadia**    was born in Zagora, Morocco in 1975. He obtained a Master's degree in Electrical Engineering from Hassan II University in 2003. He obtained the Ph.D. degree from Mohamadia School of Engineering in Rabat 2010 in Science and Technology. He is currently Professor of Electrical Engineering at CPA, CRMEF Casablanca-Settat, Morocco. Member of the Laboratory of Engineering, Industrial Management and Innovation (IMII). He can be contacted at email: elmaguiriouadia@gmail.com.



**Farchi Abdelmajid**    Ing Ph.D. in Electronic and Telecommunications Chiefs of research team Signals and Systems in Laboratory of Engineering, Industrial Management and Innovation. Educational person is responsible for the cycle engineer of telecommunications and embedded systems to the faculty of the sciences and technology of Settat, Morocco. He can be contacted at email: abdelmajidfarchi1@gmail.com.